

# Jitter Radiation In Gamma Ray Bursts and their afterglows: Emission and Self Absorption

Jared C. Workman<sup>1</sup>, Brian J. Morsony<sup>1</sup>, Davide Lazzati<sup>1</sup> and Mikhail V. Medvedev<sup>2</sup>

<sup>1</sup> JILA, University of Colorado, 440 UCB, Boulder, CO 80309-0440, USA

<sup>2</sup> Department of Physics and Astronomy, University of Kansas, Lawrence, KS 66045

25 July 2018

## ABSTRACT

Relativistic electrons moving into a highly tangled magnetic field emit jitter radiation. We present a detailed computation of the jitter radiation spectrum, including self-absorption, for electrons inside Weibel-like shock generated magnetic fields. We apply our results to the case of the prompt and afterglow emission of gamma-ray bursts. We show that jitter emission can reproduce most of the observed features with some important differences with respect to standard synchrotron, especially in the frequency range between the self-absorption and the peak frequency. We discuss the similarities and differences between jitter and synchrotron and discuss experiments that can disentangle the two mechanisms.

**Key words:** gamma rays: bursts — magnetic fields — radiation mechanisms: jitter — relativistic — non-thermal — self absorption

## 1 INTRODUCTION

The external shock model (Meszaros & Rees 1997; Piran 1999) has been very successful in the explanation of afterglow radiation in gamma-ray bursts. In this model the afterglow photons are produced by converting some of the internal energy of the burst blastwave into radiation. The radiation mechanism is supposed to be synchrotron produced by a population of relativistic electrons gyrating in a high intensity magnetic field. Synchrotron radiation is able to reproduce the spectra of some observed GRB afterglows (Wijers et al. 1999; Panaiteescu & Kumar 2001; Panaiteescu 2005), their temporal decays, their duration and their small level of linear polarization (Covino et al. 1999; Lazzati et al. 2004).

How the magnetic field is produced is, however, a matter of open debate. Compression of the interstellar magnetic field would generate a field that is not large enough to explain the observed frequencies. On the other hand, a strong magnetic field linked to the central object powering the explosion (e.g. the magnetic field of a neutron star) decays too rapidly with radius. In the standard external shock model, it is assumed that a quasi-equipartition magnetic field is generated by the shock and permeates the shocked interstellar medium (ISM) region without decaying. The fraction of energy given to the magnetic field is usually defined through  $B^2 = 8\pi\epsilon_B \rho$  where  $\rho$  is the energy density of the post-shock material and  $\epsilon_B$  is a non-dimensional parameter called the magnetic field equipartition parameter. Synchrotron radiation is also supposed to generate the prompt

emission photons. The synchrotron interpretation of prompt GRB spectra has however been unable to explain a sizable fraction of the spectra that display low-energy slopes steeper than  $\nu^{1/3}$ , i.e., harder than what is allowed by synchrotron. In addition, models in which the electrons are accelerated impulsively suffer from the cooling problem, i.e., while the cooling time of the electrons is extremely short, no sign of an aging electron population is observed in the spectra (Imamura & Epstein 1987; Crider et al. 1997; Preece et al. 1998; Ghisellini et al. 2000). In this paper we do not attempt to solve the cooling problem, and implicitly assume that it can be solved by allowing for a slow or repeated acceleration of the emitting electrons.

Particle in cell (PIC) simulations of collisionless shocks have demonstrated that the Weibel instability can produce magnetic fields at almost equipartition ( $\epsilon_B \sim 0.1$ , Silva et al. 2003; Fredriksen et al. 2004). Recent state-of-the-art PIC simulations demonstrate that the Weibel-generated magnetic fields survive for at least a few hundred skin depths (Spitkovsky 2005; Chang, et al. 2007; Spitkovsky 2007), in agreement with predictions by Medvedev, et al. (2005). Whether these fields can avoid dissipation and survive beyond the few hundred plasma skin depths remains an open question. What appears certain is that the field created by the Weibel instability has a very short coherence length, so that classical synchrotron formulae cannot be generally applied.

Radiation produced by relativistic particles in small-scale magnetic fields has been a subject of study for several decades. Historically, it begins with two seminal papers by

Landau & Pomeranchuk (1953) and Migdal (1954), who predicted the suppression of the spectral power of low-energy harmonics — the Landau-Pomeranchuk-Migdal effect. Interestingly, the spectral properties of synchrotron radiation from either homogeneous fields or from random fields coherent on scales larger than the particle Larmor radius is rather universal, as it can be straightforwardly applied in a wide variety of magnetic field configurations. In contrast to synchrotron radiation, the radiation emitted from a magnetic field (not necessarily random) whose gradient scale is smaller than the particle gyro-orbit, is determined by the particular field configuration. Therefore, one has to be very specific about the field structure in the system for which the radiation spectrum is computed.

A number of theories of radiation by relativistic electrons in small-scale magnetic fields in various regimes have been developed, including radiation in wiggler/undulator fields and free-electron lasers (presently used in sources of X-ray and extreme UV light) (Kincaid 1977; Joshi et al. 1987; Fedele et al. 1990; Williams et al. 1993; Attwood et al. 1993, Attwood 2000), radiation emitted by cosmic rays in the interstellar medium plasma turbulence if it extends to sufficiently small scales, beyond the Larmor radius of thermal electrons (Kaplan & Tsytovich 1969; Bel'kov et al 1980; Ginzburg & Tsytovich 1984; Toptygin 1985; Toptygin & Fleishman 1987ab); transition radiation in inhomogeneous plasmas (for a good review, see monograph by Ginzburg & Tsytovich 1984); synchro-Compton (or non-linear inverse Compton) radiation produced by electrons in the non-stationary field of a strong electromagnetic wave (Gunn & Ostriker 1971; Rees 1971ab; Blandford 1972); betatron radiation emitted by a particle propagating in a magnetic field of an ion current channel (somewhat analogous to a Weibel current filament; Wang, et al 2002).

Medvedev (2000) considered radiation from Weibel-generated fields, generalizing the wiggler/undulator radiation to the case of randomly distributed current filaments and associated fields as a model of a GRB shock. The spectral properties of radiation have been analytically derived, using the perturbation theory (Landau & Lifschitz 1971), for a single electron and for a power-law electron energy distribution, in the limit of a magnetic field with a very small coherence length. The theory of jitter radiation applied to the prompt emission of GRBs was shown to be able to reproduce some characteristic features, such as the steep low-energy spectrum and the sharpness of the spectral break (Medvedev 2000). The theory has been further generalized to the 3D case by Fleishman (2006b) who calls it “Diffusive Synchrotron Radiation” (DSR) and by Medvedev (2006). Jitter radiation and diffusive synchrotron radiation describe the same phenomenon: radiation from particles traveling through small scale, random magnetic fields coherent on the scale of a plasma skin depth. The primary difference in the two approaches is that Medvedev uses the perturbative approach introduced by Landau & Lifschitz (1971) whereas Fleishman applied both the perturbative treatment and a more general non-perturbative scheme which allows for the effects of scattering to appear in the spectra as the coherence length of the field increase. Fleishman (2006b) and, independently, Medvedev (2006) obtained the single electron spectrum to be  $F_\nu \propto \nu^0$  in the perturbative approach, noting the possibility that steeper spectra (up to

$\nu \propto \nu^1$ ) could be obtained if the magnetic field spectrum could be factorized. Previous results were obtained by solving the non-perturbative equation describing single electrons emitting radiation due to both large scale ordered fields and small scale random fields (Toptygin 1985; Toptygin & Fleishman 1987a). The anisotropy of jitter radiation has also been suggested as a possible explanation of the rapid spectral variability of prompt GRB emission (Medvedev 2006). Recently, the jitter radiation model has been extended to the self-absorption regime (Medvedev, et al. 2007) and applied to GRB afterglows. Approximated analytical spectra and light curves were computed.

In this paper we use the theory of jitter radiation as it is more amenable to numerical and analytical calculations (following Medvedev 2006) to improve upon the analytical computations of Medvedev et al. 2007. We review and refine the jitter theory including self-absorption, numerically implement it in a radiation code, and apply it for the optical-UV range for the prompt emission of GRBs. We also compare properties and spectral characteristics of jitter and synchrotron radiation models in the afterglow regime. We show that jitter radiation is a viable framework for the interpretation of prompt and afterglow observations. We discuss the observational implications of this alternative radiation mechanism and discuss some observational tests to compare synchrotron and jitter radiation in GRBs.

The paper is organized as follows: in § 2 we compute the emissivity of jitter radiation and the absorption coefficient, in § 3 we discuss the range over which our results are valid. In § 4 we apply our result to some cases relevant for GRB prompt and afterglow emission. We conclude in § 5 by discussing some implications for GRB observations.

## 2 SPECTRUM OF JITTER RADIATION

This section lays out the analytical framework we use to compute the specific intensity  $I_\omega$  of jitter radiation produced by Weibel generated magnetic fields. In the first part we detail how we mathematically describe the magnetic field produced by the Weibel instability and used in the calculations. In the second part we discuss the mathematical formulation used to calculate the emission coefficient  $j_\omega$ , which describes the angle-averaged power per unit frequency added to the radiation field by electrons emitting jitter radiation. Finally, the third part describes how to obtain the absorption coefficient  $\alpha_\omega$ , which describes how jitter radiation self attenuates.

As a first step we derive the absorption and emission coefficients in the comoving frame. Although we calculate the comoving quantities, it is straightforward to transform to the observer frame by recalling that  $\alpha_\omega \omega$  and  $\frac{j_\omega}{\omega^2}$  are both Lorentz invariants with  $\omega = \omega' \gamma_b (1 + \frac{v}{c} \cos \Theta')$  where  $\gamma_b$  and  $v$  refer to the bulk velocity of the object and not to the Lorentz factors of the individual emitting electrons and  $\cos \Theta'$  is defined by the angle between the photon path and the co-moving volume velocity direction. This algebraic transformation allows us to recast the equation for the observed intensity as a function of comoving quantities. Proceeding in this manner greatly simplifies the analytics and allows us to solve for the observed specific intensity by using numerically computed, comoving quantities.

## 2.1 Magnetic Fields In Gamma Ray Bursts

The standard model for emission from both the prompt burst in GRBs and the afterglow relies mainly on the assumption that the radiative mechanism is synchrotron (Zhang & Meszaros 2004; Granot et al. 1999ab). While the assumption of synchrotron is reasonable for some of the observed prompt bursts due to strong magnetic field progenitors, it is unlikely that it is always dominant in afterglow emission. Parameterizing the strength of the magnetic field by  $\epsilon_B$ , which is the ratio of the magnetic field energy density to the thermal energy density, leads to values of  $\epsilon_B$  (from observations and simulations) ranging from  $10^{-1}$  to  $10^{-5}$  (Medvedev & Loeb 1999; Panaiteescu & Kumar 2001; Panaiteescu 2005).

The field may be directly connected to the compact object powering the GRB outflow. In that case, assuming a strong field of  $\sim 10^{16}$  G on the surface of the compact object and considering volume expansion in an outflow ( $B \propto V^{-2/3}$ ), one obtains  $B \sim 10^{-2}$  G ( $\epsilon_B \sim 10^{-7}$ ) in the afterglow region ( $R \sim 10^{16}$  cm). Such a field would be too small to reproduce the observations and would decay too steeply with time. Alternatively, the magnetic field could be generated through shock compression of a pre-existing interstellar field. In that case,  $B \propto \gamma B_{ISM}$  is too weak to generate sufficiently strong fields at the afterglow shock front and results in values of  $\epsilon_B \sim 10^{-11}$  (Medvedev & Loeb 1999). With no new mechanism available to produce fields it is unlikely that synchrotron can always be the mechanism by which afterglow radiation is produced.

One very promising candidate for the origin of the magnetic field which results in afterglow emission comes from a relativistic version of the well known two-stream Weibel instability in a plasma. In the rest frame of a relativistic shock, the Weibel instability amplifies any existing magnetic field perturbations by growing current filaments out of instreaming electrons. The amplification of the current filaments is fed by the kinetic energy of the inflowing material (the ISM in the case of GRBs) and does not saturate until all of the energy in the particle distribution function anisotropy is converted into magnetic field energy. Medvedev & Loeb (1999) have shown that the field is generated in the plane of the shock and has a coherence length of order the relativistic skin depth of the shock. Further numerical studies (Noshed et al. 2003; Silva et al. 2003; Fredriksen et al. 2004) have confirmed the existence and growth of this instability. For a detailed discussion of the Weibel instability see Medvedev & Loeb (1999). The major factor that makes magnetic fields generated via the Weibel instability unique is that the correlation length of the fields is less than a Larmor radius and, as a result, the radiation generated by electrons in Weibel fields is very different from the one generated by uniform large scale fields which result in synchrotron radiation. Additionally, the field is generated in the plane of the shock and is then transported downstream as the shock propagates into the ISM. This continual generation of field is an attractive solution to the problem of how field is either generated or carried far enough downstream to produce the radiation observed in afterglows.

In this paper we adopt the model introduced by Fleishman (2006b) and Medvedev (2006) to describe the magnetic field in Fourier space. We emphasize that such a

parametrization of the field by no means incorporates all the detail and phenomenology of the fields observed in PIC simulations of collisionless shocks. However, it has the great advantage to be analytically tractable and relatively simple. Direct computations of radiation spectra can be coupled to simulations (e.g. Hededal 2005) but they are time consuming and, albeit with a very high accuracy, provide spectral calculations valid only for that particular simulation. We further note that we have explicitly excluded the presence of electric fields in our work. Hededal (2005) found that the electric fields are generated in PIC simulations and have  $\sim 10\%$  of the energy associated to the magnetic fields. He also concluded that the primary effect of electric fields was to flatten the low frequency slope. We expect the electric fields to play a secondary role in the generation of the emergent spectrum at the wavelengths we consider and as such we have simplified the analytics and numerics by excluding it.

During the initial stage of the Weibel instability, the field is generated in the plane of the shock, with  $k_{\perp} \sim$  skin depth and  $k_{\parallel} = 0$ . At this point, the parallel and transverse spectra are decoupled. Soon after saturation, secondary instabilities develop in the parallel direction thus making  $k_{\parallel} > 0$ . Since the instability develops in the parallel direction only, there is no coupling to the transverse dynamics either, at this time, so the spectra are independent. Some coupling of the transverse and parallel dynamics begins to develop at late times, when the filaments start to twist, interact with each other and merge. At this point, we shall expect that our assumption of the separability of the field spectrum becomes an approximation. This is important especially in the afterglow phase, since it has been shown that afterglow radiation has to be produced in the whole blast wave and not only behind the shock (Rossi & Rees 2003). However, as long as the current filaments are not completely intertwined to form a statistically homogeneous state, one shall expect some degree of statistical independence of the field spectra to remain. In our description, the correlation tensor for the field is given by

$$K_{\alpha\beta}(\mathbf{k}) = 4\pi C(\delta_{\alpha\beta} - n_{\alpha}n_{\beta})f_z(k_{\parallel})f_{xy}(k_{\perp}). \quad (1)$$

We assume that the field in the plane of the shock and the field in the direction of propagation can be factored from each other where  $f_{xy}(k_{\perp}) = (k_x^2 + k_y^2)^{1/2}$  describes the field in the plane of the shock,  $f_z(k_{\parallel} = k_z)$  describes the field in the direction of the shocks propagation, and  $C$  is a normalization constant. The functions used to describe the field distribution are taken from Medvedev (2006) in order to facilitate a direct comparison with the results therein and are given by

$$f_z(k_{\parallel}) = \frac{k_{\parallel}^{2\alpha_1}}{(\kappa_{\parallel}^2 + k_{\parallel}^2)^{\beta_1}}, \quad (2)$$

and

$$f_{xy}(k_{\perp}) = \frac{k_{\perp}^{2\alpha_2}}{(\kappa_{\perp}^2 + k_{\perp}^2)^{\beta_2}} \quad (3)$$

where  $\alpha_{1,2}$ ,  $\beta_{1,2}$ , and  $\kappa_{\perp,\parallel}$  are parameters used to fit the spectrum to numerical results. In this paper we have chosen  $\alpha_1 = \alpha_2$ ,  $\beta_1 = \beta_2$ , and  $\kappa_{\perp} = \kappa_{\parallel} = k_B$  of the local field. In general  $\kappa$  is a parameter determined by local quantities (Medvedev et al. 2005) but is treated as a constant in this

paper as it does not significantly alter the shape of the spectrum in the regimes under consideration.

Finally,  $C$  is fixed by the requirement that  $\int K_{\alpha\alpha}(\mathbf{k})d\mathbf{k} = \langle B^2 \rangle$  where  $\langle B^2 \rangle$  is the mean square value of the local magnetic field. This convention for  $C$  results in a normalization of

$$C = \frac{\langle B^2 \rangle}{\int f_z(k_{\parallel})k_r f_r(k_r)dk_{\parallel}dk_r} \quad (4)$$

where we have switched from Cartesian to cylindrical coordinates to simplify the integration. Unlike previous works, we have chosen to normalize the correlation tensor by the mean square value of the magnetic field in order to obtain absolute values for the luminosity of the afterglow and prompt emission.

## 2.2 Emission - $j_{\omega}$

We now calculate the emissivity of an ensemble of isotropically distributed electrons in the jitter regime. The emissivity of a power-law distributed electrons,  $N \propto \gamma^{-p}$  with a sharp low-energy cutoff  $\gamma \leq \gamma_{\min}$  has been calculated for the simple one-dimensional jitter model in the original paper by Medvedev (2000). In two separate, fully three-dimensional treatments of jitter radiation (Fleishman 2006b; Medvedev 2006) the single electron spectral power has been calculated. The ensemble emissivity is computed as a convolution of the single electron spectral power with the electron distribution. We present here, for the first time, the total radiation emitted by a distribution of electrons using the coefficients which return the true spectrum as a function of local conditions. Other than the powers on the correlation tensor describing the magnetic field (to which the radiation spectrum is relatively insensitive) every attempt has been made to keep the number of free parameters to a minimum.

The formula used to describe the angle averaged radiation emitted by a single, relativistic particle traveling through small scale magnetic fields is given (neglecting plasma dispersion which change the low frequency results to  $\propto \omega^2$ ) by (Landau & Lifshitz, 1971, section 77 p. 215)

$$\frac{dW}{d\omega} = \frac{e^2 \omega}{2\pi c^3} \int_{\omega/2\gamma^2}^{\infty} \frac{|\mathbf{w}_{\omega'}|^2}{\omega'^2} \left( 1 - \frac{\omega}{\omega'\gamma^2} + \frac{\omega^2}{2\omega'^2\gamma^4} \right) d\omega', \quad (5)$$

where  $\gamma$  is the Lorentz factor of the particle. Due to approximations used in deriving equation (5), this equation is only valid when the ratio of a particle angular deflection due to magnetic field fluctuations ( $\alpha$ ) to its relativistic beaming angle ( $\Delta\theta \sim 1/\gamma$ ) is much less than one. This approximation is expounded upon later in the paper. In keeping with Medvedev (2000) we define this ratio as

$$\delta \equiv \frac{\gamma}{k_B \rho_e} \sim \frac{\alpha}{\Delta\theta} \quad (6)$$

where  $\rho_e$  is the Larmor radius of an electron. In practice the value of  $\delta$  calculated, for our parameters, is  $\lesssim 1$ . The value of  $\delta$  enters into the integration limits in Eqs. 10 and 11 below, and setting it equal to zero there has a small effect. The effect of this assumption can be seen in Figure 4 of Medvedev (2000). Intermediate values of  $\delta$  produce an upturn in the spectrum just below the peak that disappears when  $\delta \lesssim 0.3$ . The shift in the peak frequency and the normalization, due to the change in  $\delta$ , are not lost in our computation.

The term  $|\mathbf{w}_{\omega'}|^2$  in equation (5) is the square of the Fourier transform of the acceleration field due to the Lorentz forces. Here we replace it with a volume averaged  $\langle |\mathbf{w}_{\omega'}|^2 \rangle$  by assuming a statistically homogeneous turbulence. The derivation of this term is left for the appendix and has been included for the sake of completeness (the interested reader is referred to Fleishman 2006b for the full details) and we state here the result assuming the fields described above

$$\langle |\mathbf{w}_{\omega'}|^2 \rangle = \left( \frac{e}{\gamma m_e} \right)^2 \frac{CT}{2\pi} (1 + \cos^2 \Theta') I(\Theta'), \quad (7)$$

where  $I(\Theta')$  is given by

$$I(\Theta') = \int f_z(k_{\parallel}) f_{xy}(k_{\perp}) \delta(\omega' + \mathbf{k} \cdot \mathbf{v}) d^3k, \quad (8)$$

where  $\Theta'$  is the angle between the particle velocity and the observer in the comoving frame,  $C$  is given by equation (4),  $T$  is the period for an electron traveling in Weibel fields, and  $f_z(k_{\parallel})$  and  $f_{xy}(k_{\perp})$  are given by equations (2) and (3), respectively. To evaluate the integral in equation (8) it is necessary to specify both the limits of integration and the geometry of the problem. The limits come from the nature of the magnetic fields generated by the Weibel instability. The Fourier component associated with the fastest growing mode in the Weibel instability is

$$k_{Weibel} = \frac{4\gamma_{shock}\omega_{pe}}{2^{1/4}\bar{\gamma}_e^{1/2}c}. \quad (9)$$

The factor of  $4\gamma_{shock}$  comes from the shock compression and  $\omega_{pe}^2 = \frac{4\pi e^2 n_{Ext}}{m_e}$  is the plasma frequency of the pre-shocked material (which, in the case of afterglows, corresponds to the ISM or wind density profile). While modes are initially compressed only perpendicularly to the shock plane, we make the assumption that the spatial scales are mixed by turbulence and set the inverse length scales,  $k_{\parallel}$ ,  $k_{\perp} = k_{Weibel}$ .

The geometry of the system is defined as follows: The shock is propagating in the  $z$  direction and lies in the  $x$ - $y$  plane. A particle in the shock has a velocity vector given by  $\mathbf{k} = \hat{x}k \sin \Theta' + \hat{z}k \cos \Theta'$ , this gives us  $\mathbf{k} \cdot \mathbf{v} = k_x v \sin \Theta' + k_z v \cos \Theta'$ . Medvedev (2006) presented three separate forms for  $\langle |\mathbf{w}_{\omega'}|^2 \rangle$ , corresponding to a shock viewed at 0 degrees, at  $\pi/2$ , and in between these extremes. We chose to evaluate equation (8) somewhat differently by using the properties of the delta function to integrate the correlation function in two distinct ways. By doing this we can match the asymptotic forms with two functions as opposed to three and do not suffer from numerical errors. The two forms are necessary to avoid the introduction of infinities as  $\Theta$  approaches 0 and  $\pi/2$  degrees. The two forms we use are

$$I_1(\Theta') = \int \frac{1}{|v \cos \Theta'|} f_z \left( \frac{\omega'/v}{\cos \Theta'} + k_x \tan \Theta' \right) f_{xy}(k_x) dk_x, \quad (10)$$

and

$$I_2(\Theta') = \int \frac{1}{|v \sin \Theta'|} f_z(k_z) f_{xy} \left( \frac{\omega'/v}{\sin \Theta'} + \frac{k_z}{\tan \Theta'} \right) dk_z, \quad (11)$$

where the bar in  $f_{xy}$  denotes an integration over  $k_y$ . In Fourier space, the modes that generate the field lie within a spherical annulus with radius  $k_{\perp}$  and  $k_{\parallel} \in [\delta k_{Weibel}, k_{Weibel}]$  and this sets the limits for the integrals in equations (10)

and (11). Our magnetic field model assumes that fluctuations in the magnetic field are not generated on physical scales larger than  $\sim (\delta k_{Weibel})^{-1}$  and therefore these scales are excluded from the integration region. In practice, these large scales contribute little to the overall spectrum for  $\delta \ll 1$  and this is seen by the lack of any change when we replace  $\delta k_{Weibel}$  by zero in our code.

Choosing  $v \sim c$  and switching between forms for  $\Theta' \sim \frac{\pi}{4}$  we are able to reproduce the results of Medvedev (2006). Combining equations (2), (3), (4), (5), (7), (10), and (11) and multiplying the result by  $\frac{1}{T}$  gives us

$$P(\omega) = \frac{1}{T} \frac{dW}{d\omega} : \quad (12)$$

the total energy per unit frequency and unit time, emitted by a single electron in a magnetic field with the configuration specified by Eq. 1. Unlike the case of synchrotron, where it is possible to precisely define an orbital period, the random, small scale nature of Weibel turbulence requires a more arbitrary choice for  $T$ . We follow Medvedev (2006) and Fleishman (2006b) which includes the value of the period in the magnetic field derivation (see equation (7)). By using this method,  $T$  simply disappears from the final form for  $P(\omega)$ .

The final step required to calculate the emission from a population of electrons is to choose the form for the distribution. It is standard in GRBs and other sources of non-thermal radiation to assume that the electrons follow a power law distribution

$$n'(\gamma) = K\gamma^{-p} \quad (13)$$

where  $\gamma \in [\gamma_{min}, \infty]$ ,  $K = (p-1)n'\gamma_{min}^{p-1}$  and

$$\gamma_{min} = \frac{p-2}{p-1} \frac{\epsilon_e e'}{n'm_e c^2} \quad (14)$$

The primed quantities  $n'$  and  $e'$  refer to the comoving number and energy densities and  $\epsilon_e$  is the fraction of the thermal energy in the electrons.

Combining equations (13) and (12) and integrating from  $\gamma_{min}$  to  $\infty$  yields the final result

$$P_{tot}(\omega) = \int_{\gamma_{min}}^{\infty} n'(\gamma)P(\omega)d\gamma. \quad (15)$$

It is this equation that we have numerically solved for several values of  $\Theta'$ . In order to compute  $j_\omega$  we make several assumptions. First, we assume that there is no scattering. Second we assume an isotropic electron distribution. Third, we assume that for a given point on a surface, whether it is a plane parallel slab or a spherically expanding shell, we only see the radiation due to the comoving angle aligned to the local bulk velocity. This third assumption is physically equivalent to assuming we see only 'flashlights' from different emitting regions. Finally we assume that the medium is moving ultra-relativistically and is beamed into a narrow cone of angular width  $1/\gamma$ . Using these assumptions we make the simplifying approximation that  $j_\omega = P_{tot}(\omega)\delta(\Omega - \Omega(\hat{r}))$ . Bearing in mind that we have so far calculated all quantities in the comoving frame, this form for the emissivity introduces an additional factor of  $\gamma^2(1 + \beta \cos \Theta')^2$  when transforming to the observer's frame due to the transform of the solid angle (Granot, Piran, & Sari 1999a; Rybicki & Lightman 1979).

In order to check our results we have performed the following tests. First, it can be shown analytically (for  $\beta_{1,2} = 0$ ) that combining the  $\Theta' = 0$  form of  $\langle |\mathbf{w}_{\omega'}|^2 \rangle$  with  $P = (2e^2\gamma^4/3c^3)(w_\perp^2 + \gamma^2 w_\parallel^2)$  (equation 4.92 of Rybicki & Lightman 1979) Eq. 12 reduces to

$$dW/dt = (2/3)r_e^2 c \gamma^2 \langle B^2 \rangle, \quad (16)$$

which is equivalent to the case of synchrotron radiation. We have confirmed that our procedure numerically returns the same value by integrating equation (5). Setting  $\beta_{1,2} \neq 0$  in our code does not change this result. Second, we replaced  $P(\omega)$  in equation (15) with the the form for synchrotron radiation and verified that our technique yielded results which were in agreement with the analytic form for  $P_{tot,Synch}(\omega)$  given by equation 6.36 in Rybicki & Lightman (1979).

### 2.3 Absorption - $\alpha_\omega$

Given the single particle emissivity,  $P(\nu)$ , and the particle energy distribution, the calculation of the jitter self-absorption is straightforward. We have analytically calculated it (Medvedev, et al. 2007) in the regimes when the self-absorption frequency is above and below the jitter peak frequency. For numerical implementation, the self-absorption coefficient  $\alpha_\omega$  can be derived using equation 6.50 from Rybicki & Lightman (1979) as follows:

$$\alpha_\nu = -\frac{c^2}{8\pi\nu^2} \int P(\nu, E)E^2 \frac{\partial}{\partial E} \left[ \frac{N(E)}{E^2} \right] dE \quad (17)$$

Using  $P(\nu, E) = 2\pi P(\omega)$ ,  $E = \gamma m_e c^2$ ,  $N(E) = \frac{d\gamma}{dE} n(\gamma)$ , and  $\omega = 2\pi\nu$  where  $n(\gamma)$  and  $p(\omega)$  are given by equations (12) and (13), quickly yields

$$\alpha_\omega = \frac{(p+2)\pi^2 k}{m_e \omega^2} \int_{\gamma_{min}}^{\infty} \gamma^{-(p+1)} P(\omega) d\gamma. \quad (18)$$

Effectively, once the numerical problem of solving equation (15) has been solved, the only modification necessary to obtain the absorption coefficient is a change in the power on gamma and a change in the normalization constant. In using this form for the absorption coefficient we have assumed that the electron distribution is locally isotropic, that no scattering occurs, and that the local absorption is dominated by electrons moving with only one angle with respect to the observers line of sight. For a further discussion of the absorption coefficient see Medvedev et al. (2007).

## 3 LIMITATIONS OF VALIDITY

Equation (5) is derived using the perturbation theory (Landau & Lifshitz 1971) and, consequently, has a limited range of applicability. Jitter radiation explicitly assumes that the coherence length of the emission is small enough that the approximation of rectilinear motion is valid (Medvedev 2000 & Fleishman 2006b). The coherence length  $\lambda_c$  is proportional to  $1/\omega$  and clearly increases as the frequency decreases. Fleishman (2006) describes that, at lower frequencies, a particle trajectory random walks due to repeated scatterings off magnetic field inhomogeneities. This scattering results in a modification of the emitted radiation in the region of

the spectrum just before where the plasma dispersion dominates. The non-perturbative version of the theory of radiation emitted in small scale field (Toptygin & Fleishman 1987, Fleishman 2006a) accounts for this effect and finds a  $P(\omega) \propto \omega^{\frac{1}{2}}$  regime in this region. At even lower frequencies,  $\omega \lesssim \omega_{pi}$ , the spectrum follows  $P(\omega) \propto \omega^2$  due to plasma dispersion. This region is at photon energies of a fraction of an eV or less in prompt GRBs and at frequencies below  $\sim 1$  MHz in afterglows, assuming standard GRB parameters.

The perturbative form of the theory fully accounts for the spectrum above and below (down to the plasma dispersion regime) the  $P(\omega) \propto \omega^{\frac{1}{2}}$  region. For the purposes of this work it can be shown that the region in frequency (approximately) given by  $\omega < \epsilon_B \omega_{jm}$  (where  $\omega_{jm}$  is the peak frequency of jitter radiation for a given minimum Lorentz factor) is affected by scattering and therefore the spectrum obtained with the methods used in this paper is only approximate. This limitation does not pose a problem for this work. It can be shown that  $\delta \approx 36\sqrt{\epsilon_B}$  (Medvedev et al. 2007) which requires we assume  $\epsilon_B < 10^{-3}$  and, more realistically, in the range of  $10^{-6} - 10^{-4}$ . Even for a value of  $\epsilon_B = 10^{-2}$  the cutoff frequency  $\epsilon_B \omega_{jm}$  corresponds to an energy at the edge of the BATSE cutoff window of 20 keV.

The only case in which the limitations of the perturbation approach may be relevant is the modeling of the afterglow spectrum. Even in such a case, however, the region in question generally lies entirely within or close to the optically thick portion of the spectrum, in which case the spectrum simplifies to the source function. In cases where the spectrum generated by our perturbative approach may be incorrect we will note it in the individual results.

## 4 RESULTS

We here consider a single internal shock within the prompt phase of a GRB. The material has a pre-shock density of  $9.25 \times 10^{-12}$  g/cm<sup>3</sup>, a shock Lorentz factor of  $\gamma_{int} = 2$ ,  $\epsilon_e = 0.2$ , and a magnetic equipartition fraction<sup>1</sup>  $\epsilon_B = 10^{-5}$ . The spectral index of the electrons is  $p = 2.5$ . The thickness of the shell is  $3 \times 10^6$  cm in the observer frame and the material is moving with a bulk Lorentz factor of 100. We consider a shell radiating at  $R = 3.2 \times 10^{14}$  cm. This setup corresponds to an isotropic energy of  $5 \times 10^{52}$  ergs in the shell.

These values are chosen to give a peak frequency of about 200 keV in the observer frame. The parameters describing the magnetic field distribution do not affect the spectral characteristics as long as  $\alpha_{1,2} > 0.5$  and  $\beta_{1,2} > \alpha_{1,2} + p/2$ . To be consistent with Medvedev (2006) we set  $\alpha_{1,2} = 2$ . and  $\beta_{1,2} = 10$ . It is important to keep in mind that the emission angles correspond to co-moving angles. The results plotted are the observed quantities as a function of co-moving emission angle.

Figure 1 shows the emissivity vs. frequency for different emission angles ( $\theta'$ ). For  $\theta' = 0$  the emission has a slope  $\alpha_\nu = 1$  at low frequencies and then turns over to a slope

$\alpha_\nu = -(p - 1)/2 = -0.75$ , set by the electron power index. As the angle increases, the low frequency slope near the peak decreases, and at much lower frequencies the slope flattens to  $\alpha_\nu = 0$ . Beyond an angle of 30°, there is no longer a peak in the spectrum, just a transition from a constant ( $\alpha_\nu = 0$ ) to  $\alpha_\nu = -0.75$ . The value of the low frequency constant changes with angle, peaking at 45°. At high frequencies, the slope is always the same but the emissivity at a given frequency decreases with angle. These results are in full agreement with the single electron spectra of Medvedev (2006). Figure 2 shows the absorption coefficient  $\alpha$  for the same setup. The absorption coefficient is proportional to  $P(\omega) \times \omega^{-2}$  below the peak frequency and to  $P(\omega) \times \omega^{-2.5}$  above the peak frequency.

Below frequencies of  $\sim 3 \times 10^{-3}$  eV our perturbative approach is no longer valid. A non-perturbative approach would be needed to properly calculate radiation at lower frequencies (Fleishman 2006b). Therefore, frequencies in this regime are not considered in this paper.

With  $P(\omega)$  and  $\alpha$  we can solve the 1D radiative transfer equation to find the specific intensity of the shell at different angles. Assuming the observable portion of the shell is spherical and that the amount of time any piece of the shell is radiating is short compared to the time it takes the shell to become visible (i.e., we assume the shell is infinitely thin), the specific intensity at a given angle is proportional to the total emission at the time that angle comes into view. Figure 3 shows the integrated specific intensity at different angles for jitter radiation. Figure 4 shows synchrotron radiation for identical conditions and angles.

The synchrotron radiation spectrum shows no change in the shape of the spectrum. The peak frequency decreases by about a factor of 2 and the power decreases by a factor of  $\sim 16$  between 0° and 90° due to relativistic effects. Jitter radiation, on the other hand, shows a large change in spectral index and total emission below the peak frequency and a decrease in emission of about a factor of  $\sim 27.5$  with angle above the peak frequency. Note that the source function for jitter and synchrotron are the same for identical conditions. Self absorption becomes important at a few 10s of eV in this example.

The time at which different angles come into view is found from the geometric time delay to be  $(1 - \cos \theta) \times r/c$  where  $\theta$  is the emission angle in the observer frame,  $r$  is the emission radius ( $10^{14}$  cm in this example) and  $c$  is the speed of light. Figure 5 shows intrinsic brightness vs. time at 10, 100, and 1000 keV and 1 eV (124 nm). At 1000 keV, above the initial peak frequency, the emission decreases with time by a factor of about 46 between  $t = 0$  and  $t = 2.1$ . At 100 keV, just below the initial peak frequency, the emission increases slightly for 0.1 s and then decreases. At 10 keV the emission increases by a factor of 7 in 0.25 s, corresponding to 40°, and then decreases. The initial amount of increase is larger at lower energies. At 1 eV, there is an initial sharp increase. Very early on, however, the emission becomes optically thick and begins a shallow decrease (by a factor of only  $\sim 7$  with time). This behavior has important implications for the interpretation of spectral lags and the optical emission during the prompt phase. As is clear from Fig. 5, the optical and high energy bands can show very little correlation, even if they come from the same electrons and the same emission mechanism. Lack of correlation was used as

<sup>1</sup> We note that there is no experimental value for the value of  $\epsilon_B$  during the prompt phase.

an argument in favor of a reverse shock origin of the optical flash in GRB 990123 (Akerlof et al. 1999, Sari et al. 1999). The flattening of the spectra in the X-ray band could also explain the soft X-ray excesses detected in some events (Preece et al. 1996; Strohmayer et al. 1998).

Figure 6 shows the ratio of the total number of photons between 110 and 320 keV to the number of photons between 55 and 110 keV vs. time. This ratio is equivalent to the count ratio of BATSE channels 3:2 (HR<sub>3/2</sub>). This plot shows a hard to soft evolution for the first 0.4 s (out to a 45° angle) and then a fairly flat hardness ratio after this.

Let us now consider the external shock phase. For an example comparison of the afterglow spectrum for jitter and synchrotron radiation we examine an isotropic explosion with an energy of 10<sup>53</sup> ergs expanding into a medium with a density of 1 particle/cm<sup>3</sup> at the observed time  $t = 1000$  s. The Blandford-McKee (Blandford & McKee, 1976) solution for a relativistic fireball is used to determine the density ( $\sim 100$  cm<sup>-3</sup>), internal energy ( $\sim 4$  erg cm<sup>-3</sup>) and Lorentz factor ( $\Gamma \sim 25$ ) of the material at the leading edge of the shock. A thin shock model is used to calculate the emission and the optical depth. A magnetic field equipartition parameter  $\epsilon_B = 10^{-5}$  and an electron equipartition parameter  $\epsilon_e = 0.01$  are assumed everywhere, and a shock thickness of  $\frac{r}{2\gamma^2} \approx 2.4 \times 10^{14}$  cm everywhere is assumed. Figure 7 shows a comparison between the emission from jitter and synchrotron radiation under these conditions. Below the peak frequency, the synchrotron emission increases with frequency as  $\nu^{1/3}$ , while the jitter spectrum is nearly flat. This is due to the fact that large angles dominate the afterglow spectrum (see also Medvedev et al. 2007). The synchrotron and jitter spectra become optically thick at around 10<sup>-4</sup> eV (24 GHz) and 10<sup>-3</sup> eV (240 GHz), respectively, in this example, but this is dependent on the thickness of the afterglow material.

## 5 SUMMARY AND DISCUSSION

We have computed jitter radiation spectra for a non-thermal population of relativistic electrons radiating in a highly non-uniform magnetic field, including self absorption. Our results are in agreement, when relevant, with previous computations (Fleishman 2006b; Medvedev 2006; Medvedev, et al. 2007). Due to the complexity of the problem, several assumption and/or simplification were made in order to obtain a semi-analytical result for the spectra. We here review the assumptions and simplifications made.

- The most important simplification we adopt is that of assuming that the field can be factorized in the parallel and perpendicular directions with respect to the shock propagation velocity. This assumption is fundamental in our results as it allows for the dependence of the low-frequency spectral slope on the viewing angle. It is likely to be a good assumption immediately behind the shock and become progressively worse as the ion current filaments get twisted and/or merge, mixing the parallel and perpendicular components of the field.

- The strength of the magnetic field is assumed to be uniform throughout the shocked region and the average magnetic field to be rather small (containing only a fraction

$\sim 10^{-5}$  of the internal energy of the blast wave). Such assumption is necessary to simplify the computation and to make sure the radiation is produced in the jitter regime rather than in a transition region. PIC simulations (Silva et al. 2003; Fredriksson et al. 2004; Cheng et al. 2007) find a stronger magnetic field right behind the shock and a moderate decline behind it. However, PIC simulations can follow the shocked material only several hundred skin depths behind the shock, while afterglow radiation has to be produced by the whole blast wave, in order to avoid a strong inverse Compton component that is not observed (Rossi & Rees 2003).

- The peak of the magnetic spectrum can be around the ion skin length and this seems to invalidate the jitter condition for leptons. However, this does not invalidate the use of jitter radiation, because the deflection angle depends on the product of the field correlation length and the field strength. We took this into account: the jitter break will be above the synchrotron frequency in the field of the same strength if  $\epsilon_B \lesssim 10^{-3}$ . Fits to observational data of GRBs favor such low values (Panaitescu & Kumar 2001; Table 3 of Panaitescu 2005). If the field strength is larger, the jitter regime transforms into the wiggler regime (Attwood 2000) and, for even stronger fields and larger correlation lengths - into the synchrotron regime. We should also stress here that in reality the magnetic field spectrum spans at least several decades in  $k$ -space, with the highest  $k$  being even higher than  $\omega_{pe}/c$ , even for the electron-ion plasmas (Wiersma & Achterberg 2004). This is also confirmed in PIC simulations. Radiation from these fields will surely be in the jitter regime; the low- $k$  part of the field spectrum will produce synchrotron-like radiation, as is discussed in (Medvedev 2000).

- Our computations are performed in the perturbative approach and cannot be applied in some regimes. Especially relevant is the low frequency range where the photons scatters off the magnetic field inhomogeneities resulting in a  $F(\nu) \propto \nu^{1/2}$  regime (Fleishman 2006b).

- Simulation of magnetic field generation in ion-electron collisionless shocks find evidence of electric fields on top of magnetic fields. We neglect the acceleration of the electrons due to electric fields in our computations. A discussion of the effect of electric fields can be found in Hededal 2005, who conclude that the effect is that of flattening the low frequency slope. This effect will be important in the modeling of the prompt bursts but not in afterglows, where the resultant spectrum will be dominated by the limb.

- We also assume that there is no correlation between the electron energy and the magnetic field locally. Such assumption is customary also for synchrotron computations.

- Finally, the limit  $\delta \ll 1$  is assumed

We find that depending on the orientation of the line of sight with respect to the shock front the jitter spectrum is different. For shocks observed head on, the spectrum is peaked, with a steep low energy slope  $F(\nu) \propto \nu$ . For shocks observed edge on, the spectrum at the left of the peak is flat down to the self absorption frequency or to the frequency at which scattering off the magnetic field inhomogeneities becomes important (Fleishman 2006b). We applied these results to standard GRB cases, for the prompt and for the afterglow emission. We find that, in addition to some of the observations already discussed in the previous literature

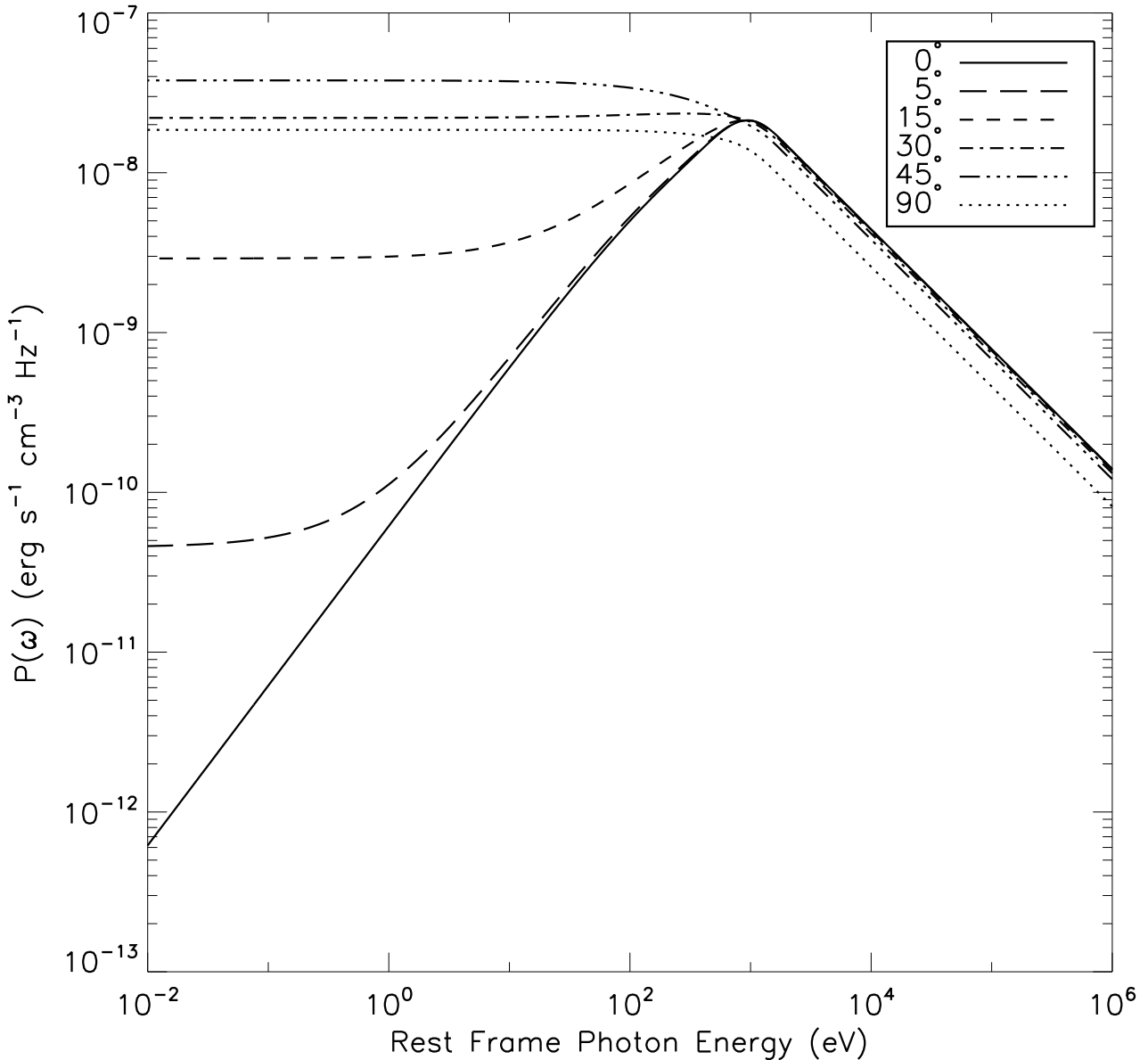


**Figure 1.** Jitter emissivity vs. frequency at different angles between the bulk velocity vector and the line of sight. The angles plotted are  $\theta' = 0^\circ$  (solid line),  $5^\circ$  (long-dashed line),  $15^\circ$  (dashed line),  $30^\circ$  (dot-dash line),  $45^\circ$  (3 dot-dash), and  $90^\circ$  (dotted line). All the angles are measured in the comoving frame.

(Medvedev 2000, 2006), jitter radiation can explain X-ray excesses in the prompt spectrum and the lack of correlation between optical and high energy radiation. This is due to the fact that the optical radiation lies in the regime where the spectral slope depends on the orientation angle, while the high energy emission depends only on parameters that do not evolve with time. We also find that jitter radiation explains naturally the presence of spectral lags (Norris et al. 2001).

In the afterglow regime, the optical and X-ray spectra are very similar to those of synchrotron radiation. At frequencies below the peak, differences are instead clearly visible. First, the spectrum is flat ( $F(\nu) \propto \nu^0$  instead of

$F(\nu) \propto \nu^{1/3}$ ); second, the self absorption frequency is at higher frequencies (see also Medvedev, et al. 2007 who also show that self absorption frequency has a different temporal evolution in jitter and synchrotron). Understanding the implications of those differences is not simple and a proper fit has to be performed (Morsony et al. in preparation). It is likely that jitter spectra fit to afterglow data will give different results in term of the properties of the ambient medium, since radio observations are always very important in constraining the density of the interstellar material. A more detailed discussions will be possible only after a formal fit has been performed.

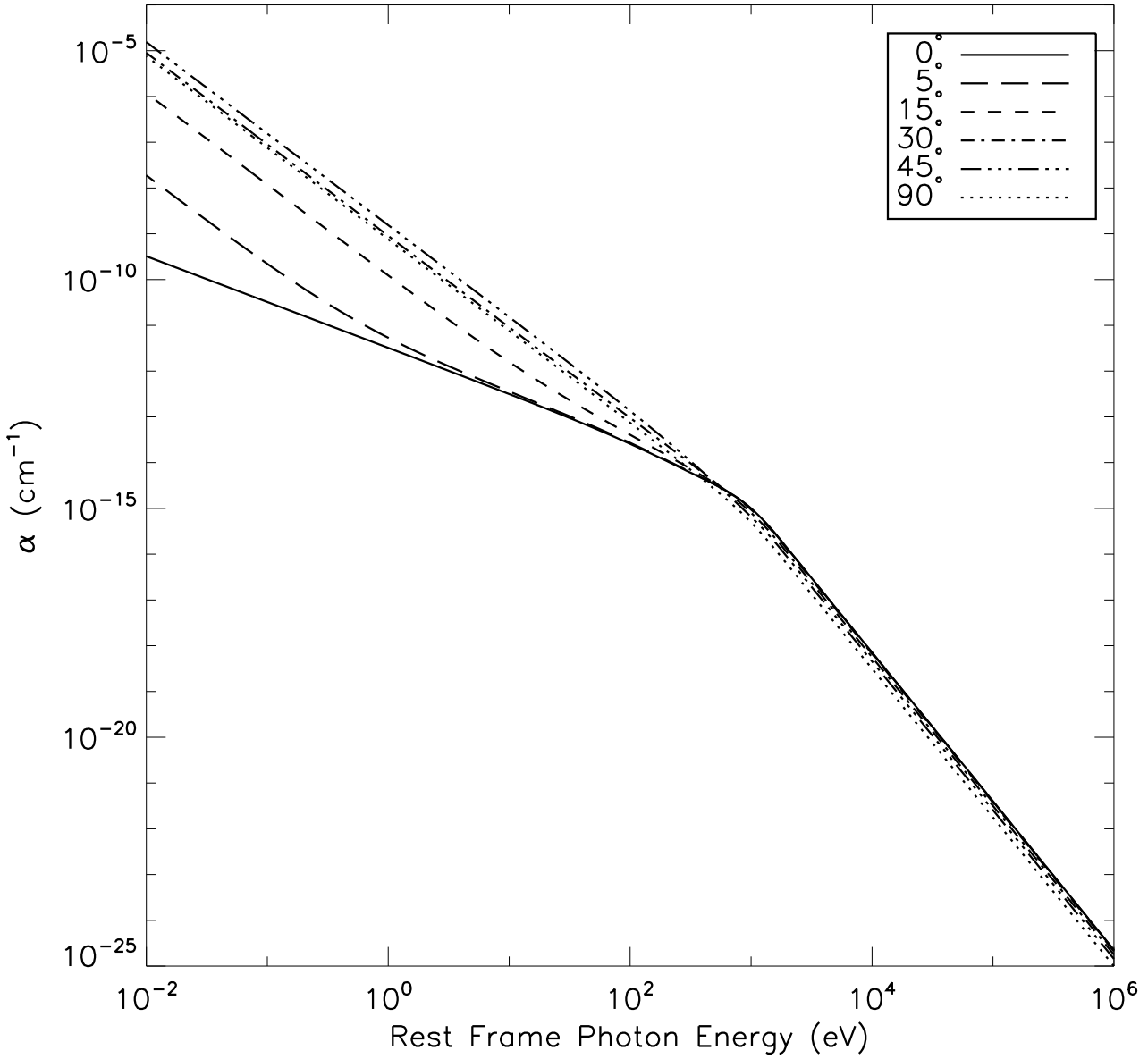


**Figure 2.** Absorption coefficient  $\alpha$  vs. frequency at different angles between the bulk velocity vector and the line of sight. The angles plotted are  $\theta' = 0^\circ$  (solid line),  $5^\circ$  (long-dashed line),  $15^\circ$  (dashed line),  $30^\circ$  (dot-dash line),  $45^\circ$  (3 dot-dash), and  $90^\circ$  (dotted line).

## ACKNOWLEDGEMENTS

This work was supported by NSF grants AST-0407040 (JW) and AST-0307502 (BM, DL), NASA Astrophysical Theory Grants NNG04GL01G and NNX07AH08G (JW), NNG06GI06G (BM, DL) and NNG-04GM41G (MM), Swift Guest Investigator Program grants NNX06AB69G (BM, DL) and NNX07AJ50G (MM), and DoE grant DE-FG02-04ER54790 (MM). MM gratefully acknowledges support from the Institute for Advanced Study.

## REFERENCES

Akerlof C., et al., 1999, *Nature*, 398, 400

Attwood, D., et al. 1993, *Appl. Opt.*, 32, 7022  
 Attwood, D., 2000, *Soft X-ray and extreme ultraviolet radiation: principles and applications* (Cambridge Univ. Press: New York)  
 Bel'kov, S.A., Nikolaev, Y.A., Tsytovich, V.N. 1980, *Sov. Radiophys.*, 23, 181  
 Blandford, R.D. 1972, *Astron. Astroph.* 20, 135  
 Blandford, R. D., & McKee, C. F. 1976, *Physics of Fluids*, 19, 1130  
 Chang, P., Spitkovsky, A., Arons, J. 2007, *ApJ*, submitted, arXiv:0704.3832  
 Covino S., et al., 1999, *A&A*, 348, L1  
 Crider A., et al., 1997, *ApJ*, 479, L39  
 Ferede, R., et al. 1990, *Phys. Scr.*, 30, 192  
 Fleishman, G. D. 2006a, in *High-Frequency Waves in Geospace*,

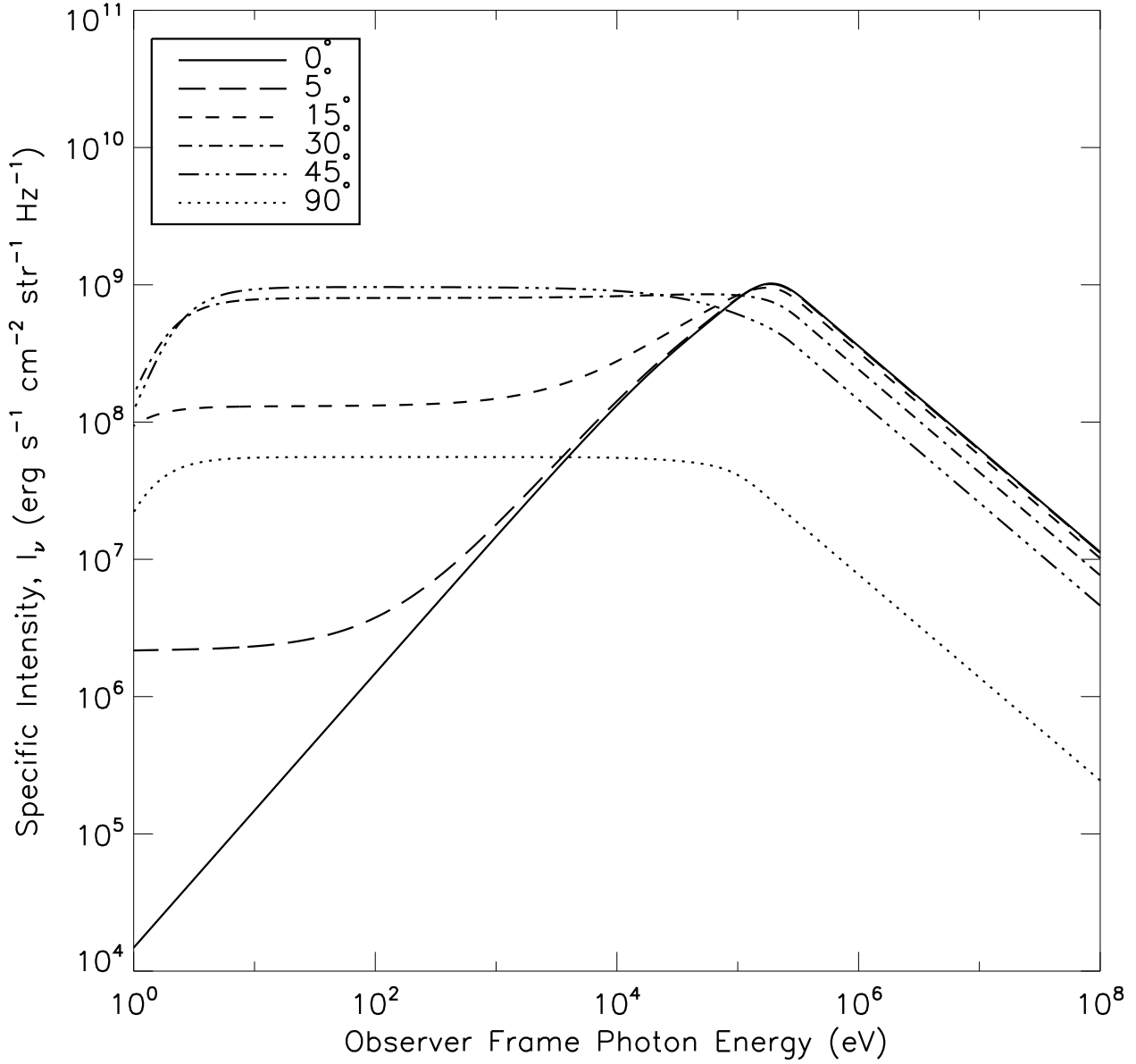


**Figure 3.** Jitter emission of a single relativistic shell as seen from different angles (angles measured in the comoving frame). The angles plotted are  $\theta' = 0^\circ$  (solid line),  $5^\circ$  (long-dashed line),  $15^\circ$  (dashed line),  $30^\circ$  (dot-dash line),  $45^\circ$  (3 dot-dash), and  $90^\circ$  (dotted line). Jitter radiation peaks at about 190 keV.

ed. J. Labelle & R. Treumann (Berlin: Springer), 83  
 Fleishman, G. 2006b, ApJ, 638, 348  
 Frederiksen, J., Hededal, C., Haugbølle, T. & Nordlund, Å., 2004, ApJ, 608, L13  
 Ghisellini G., Celotti A., Lazzati D., 2000, MNRAS, 313, L1  
 Ginzburg, V.L. & Tsytovich, V.N. 1984, The transition radiation and transition scattering (Moscow, Russia: Nauka)  
 Granot, J., Piran, T., & Sari, R. 1999a, ApJ, 513, 679  
 Granot, J., Piran, T., & Sari, R. 1999, ApJ, 527, 236  
 Gunn, J.E. & Ostriker, J.P. 1971, ApJ, 157, 1395  
 Hededal, C., 2005, Ph.D. thesis (astro-ph/0506559)  
 Imamura J. N., Epstein R. I., 1987, ApJ, 313, 711  
 Joshi, C., et al. 1987, IEEE J. Quantum Electron., 23, 1573  
 Kaplan, S.A., & Tsytovich, V.N. 1969, Sov. Phys. Uspekhi, 97,

77 (Usp. Fiz. Nauk, 97, 77)  
 Kincaid, B.M. 1977, J. Appl. Phys., 48, 2684  
 Landau, L. D., & Lifshitz, E.M. 1971, The Classical Theory of Fields (Oxford: Pergamon Press)  
 Landau, L.D. & Pomeranchuk 1953, Sov. Phys. Doklady, 92, 535 (Dokl. Akad. Nauk SSSR, Ser. Fiz. 92, 535)  
 Lazzati D., et al., 2004, A&A, 422, 121  
 Medvedev, M. V. 2000, ApJ, 540, 704  
 Medvedev. M.V. 2005, astro-ph/0503463  
 Medvedev, M. V. 2006, ApJ, 637, 869  
 Medvedev, M. V., & Loeb, A. 1999, ApJ, 526, 697  
 Medvedev, M. V., Fiore, M., Fonseca, R., Silva, L. O., & Mori, W. 2005, ApJ, 618, L75  
 Medvedev, M. V., Lazzati, D., Morsony, B. C., & Workman, J.

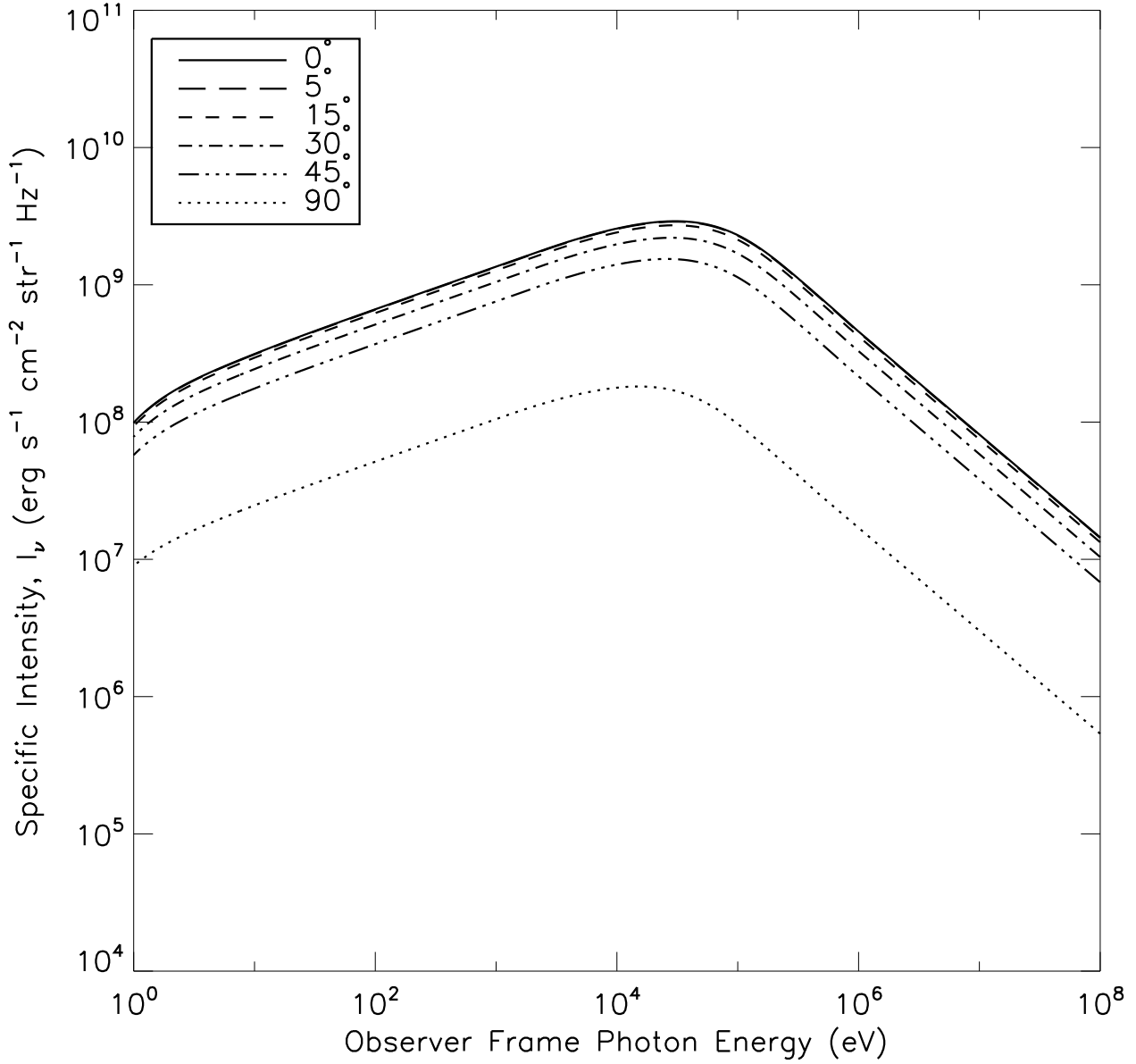


**Figure 4.** Synchrotron emission for a single relativistic shell at different angles (analogous to Fig. 3). The angles plotted are  $\Theta' = 0^\circ$  (solid line),  $5^\circ$  (long-dashed line),  $15^\circ$  (dashed line),  $30^\circ$  (dot-dash line),  $45^\circ$  (3 dot-dash), and  $90^\circ$  (dotted line). Synchrotron radiation peaks at about 31 keV

C., 2007, 666, 339  
 Meszaros P., Rees M. J., 1997, ApJ, 476, 232  
 Migdal, A.B. 1954, Sov Phys. Doklady, 94, 1033 (Dokl. Akad. Nauk SSSR, 94, 1033)  
 Nishikawa, K.-I., Hardee, P., Richardson, G., Preece, R., Sol, H., & Fishman, G. J. 2003, ApJ, 595, 55  
 Panaiteescu A., Kumar P., 2001, ApJ, 554, 667  
 Panaiteescu A., 2005, MNRAS, 363, 1409  
 Piran, T. 1999, Physics Reports, Volume 314, Issue 6, 575  
 Preece R. D., Briggs M. S., Pendleton G. N., Paciesas W. S., Matteson J. L., Band D. L., Skelton R. T., Meegan C. A., 1996, ApJ, 473, 310  
 Preece R. D., Briggs M. S., Mallozzi R. S., Pendleton G. N., Paciesas W. S., Band D. L., 1998, ApJ, 506, L23  
 Rees, M.J. 1971a, Nature, 229, 312  
 Rees, M.J. 1971b, Nature, 230, 55  
 Rossi E., Rees M. J., 2003, MNRAS, 339, 881  
 Rybicki, G. B., & Lightman, A. P. 1979, Radiative Processes in Astrophysics, (New York: Wiley)  
 Sari R., Piran T., Halpern J. P., 1999, ApJ, 519, L17  
 Silva, L. O., Fonseca, R. A., Tonge, J. W., Dawson, J. M., Mori, W. B., & Medvedev, M. V. 2003, ApJ, 596, L121  
 Spitkovsky, A. 2005, AIP Conf. Proc., 801, 345; arXiv:astro-ph/0603211  
 Spitkovsky, A. 2007, ApJL, submitted  
 Strohmayer T. E., Fenimore E. E., Murakami T., Yoshida A., 1998, ApJ, 500, 873  
 Toptygin, I.N. 1985, Cosmic rays in interplanetary magnetic

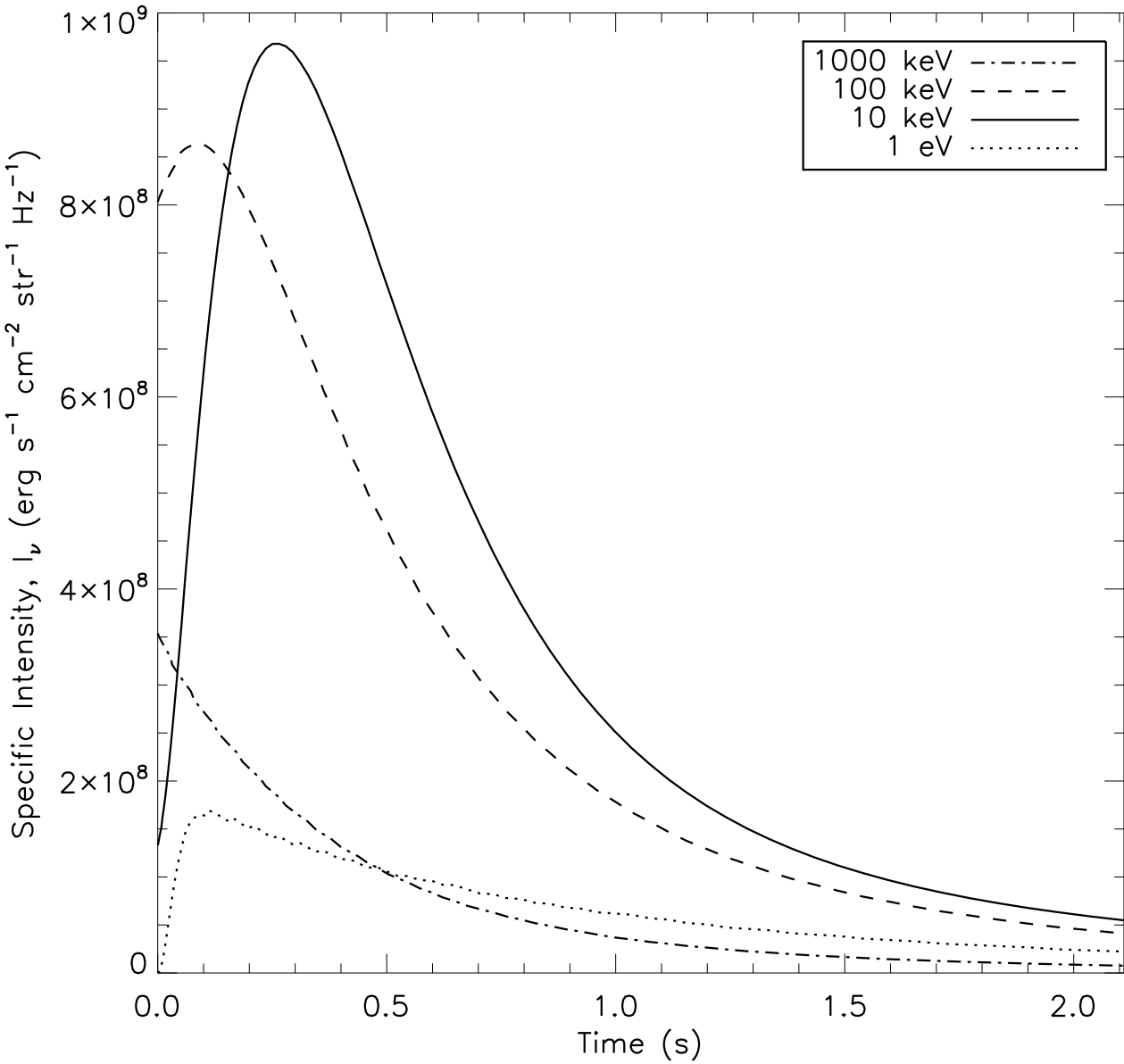


**Figure 5.** Jitter radiation light curves for a single thin relativistic shell at 1 MeV (dot-dash line), 100 keV (dashed line), 10 keV (solid line) and 1 eV (dotted line).

fields, (Dordrecht, Netherlands: D. Reidel Publ. Co.)  
 Toptygin, I. N., & Fleishman, G. D. 1987a, Ap&SS, 132, 213  
 Toptygin, I. N. & Fleishman, G. D. 1987b, Radiophys. Quantum Electron., 30, 551  
 Wang, S., et al. 2002, PRL, 88, 135004-1  
 Weibel, E. S. 1959, Phys. Rev. Lett., 2, 83  
 Wiersma J., Achterberg A., 2004, A&A, 428, 365  
 Wijers R. A. M. J., Galama T. J., 1999, ApJ, 523, 177  
 Williams, R.L., et al. 1993, IEEE Trans. Plasma Sci., 21, 156  
 Zhang, B. & Mészáros 2004, International Journal of Modern Physics, 19, 2385

#### APPENDIX A: DERIVATION OF $\langle |\mathbf{W}_{\omega'}|^2 \rangle$

The following derivation is directly derived from Medvedev (2006) and Fleishman (2006b) and is included for the sake of completeness. First, let us define a parameter  $\delta$  which defines the ratio of deflection ( $\alpha$ ) due to Lorentz forces and beaming ( $\Delta\theta$ ) due to relativistic effects experienced by a particle moving with Lorentz factor  $\gamma$  in a small scale, random magnetic field with a typical correlation length,  $k_B$  and Larmor radius,  $\rho_e$ .

$$\delta \equiv \frac{\gamma}{k_B \rho_e} \sim \frac{\alpha}{\Delta\theta} \quad (\text{A1})$$

For values of  $\delta \ll 1$  the particle trajectory is nearly a straight line (with small perpendicular motions introduced by the

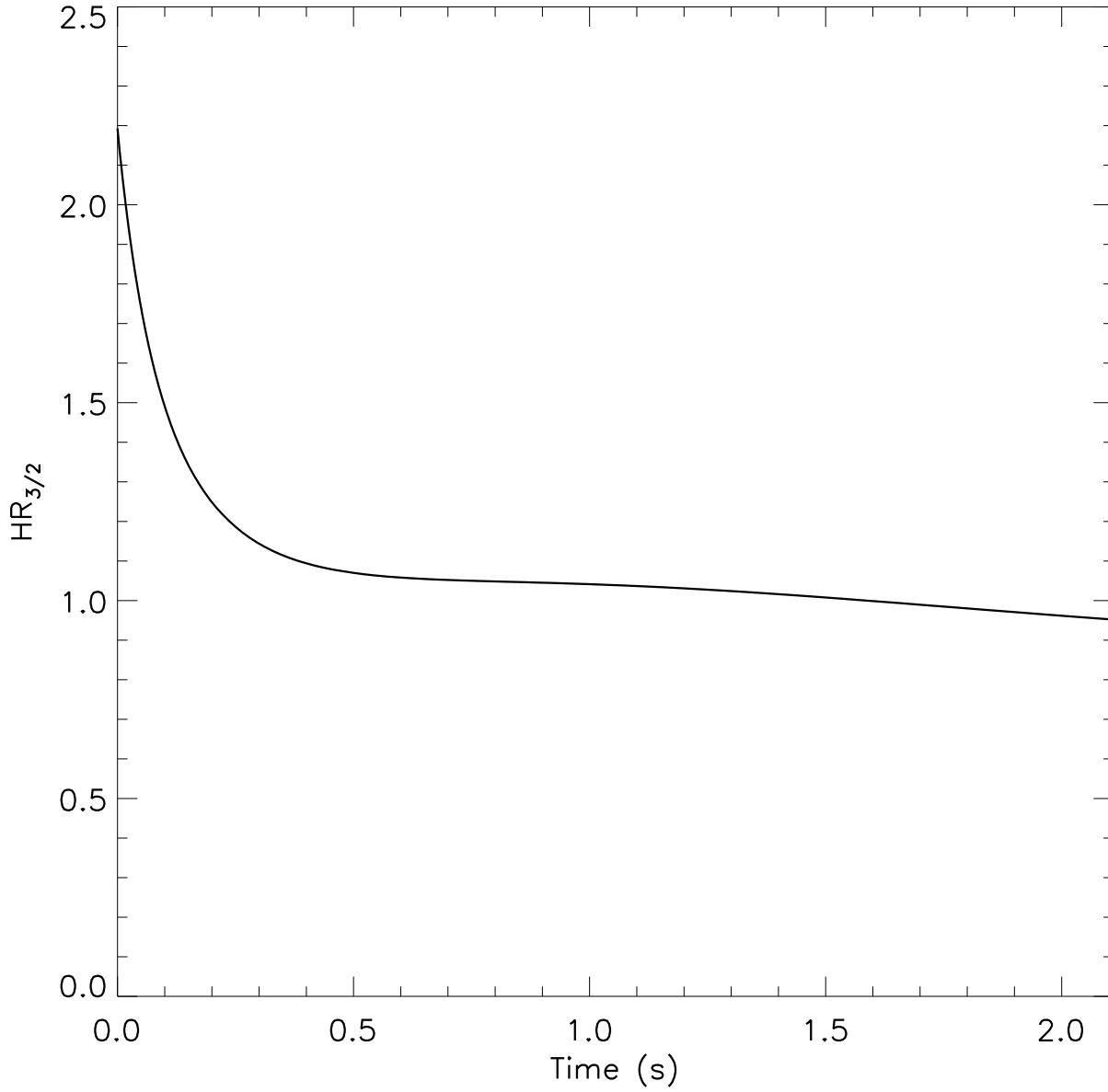


**Figure 6.** Simulated BASTE 3:2 channel hardness ratio vs. time.  $HR_{3/2}$  is defined as the ratio of the number of photons between 110 and 320 keV to the number of photons between 55 and 110 keV.

Lorentz forces). In this case the angle averaged spectral energy, neglecting plasma dispersion, is given by Landau & Lifshitz (1971, section 77, p. 215):

$$\frac{dW}{d\omega} = \frac{e^2 \omega}{2\pi c^3} \int_{\omega/2\gamma^2}^{\infty} \frac{|\mathbf{w}_{\omega'}|^2}{\omega'^2} \left( 1 - \frac{\omega}{\omega' \gamma^2} + \frac{\omega^2}{2\omega'^2 \gamma^4} \right) d\omega' \quad (\text{A2})$$

where  $\mathbf{w}_{\omega'}$  is the Fourier transform of the transverse acceleration of the particle due to Lorentz forces ( $\mathbf{w} \equiv F_L/\gamma m$ ). Fourier transforming the acceleration field along a particles trajectory  $\mathbf{w}(\mathbf{r}_0 + \mathbf{v}t, t)$  yields

$$\mathbf{w}_{\omega'} = (2\pi)^{-4} \int e^{i\omega' t} dt (e^{-i(\Omega t - \mathbf{k} \cdot \mathbf{r}_0 - \mathbf{k} \cdot \mathbf{v}t)} \mathbf{w}_{\Omega, \mathbf{k}} d\Omega d\mathbf{k})$$

$$= (2\pi)^{-3} \int \mathbf{w}_{\Omega, \mathbf{k}} \delta(\omega' - \Omega + \mathbf{k} \cdot \mathbf{v}) e^{i\mathbf{k} \cdot \mathbf{r}_0} d\Omega d\mathbf{k}. \quad (\text{A3})$$

Squaring the above result and averaging over volume using the results  $\langle |\mathbf{w}_{\omega'}|^2 \rangle = V^{-1} \int |\mathbf{w}_{\omega'}|^2 d\mathbf{r}_0$  and  $\int e^{i(\mathbf{k} - \mathbf{k}_1) \cdot \mathbf{r}_0} d\mathbf{r}_0 = (2\pi)^3 \delta(\mathbf{k} - \mathbf{k}_1)$  yields

$$\langle |\mathbf{w}_{\omega'}|^2 \rangle = (2\pi)^{-3} V^{-1} \int |\mathbf{w}_{\Omega, \mathbf{k}}|^2 \delta(\omega' - \Omega + \mathbf{k} \cdot \mathbf{v}) d\Omega d\mathbf{k}. \quad (\text{A4})$$

In the absence of electric fields<sup>2</sup> the Lorentz acceleration is given by  $(e/\gamma mc)\mathbf{v} \times \mathbf{B}$  which, in tensor notation, is

<sup>2</sup> See § 2.1 for a discussion on the implications of this assumption.

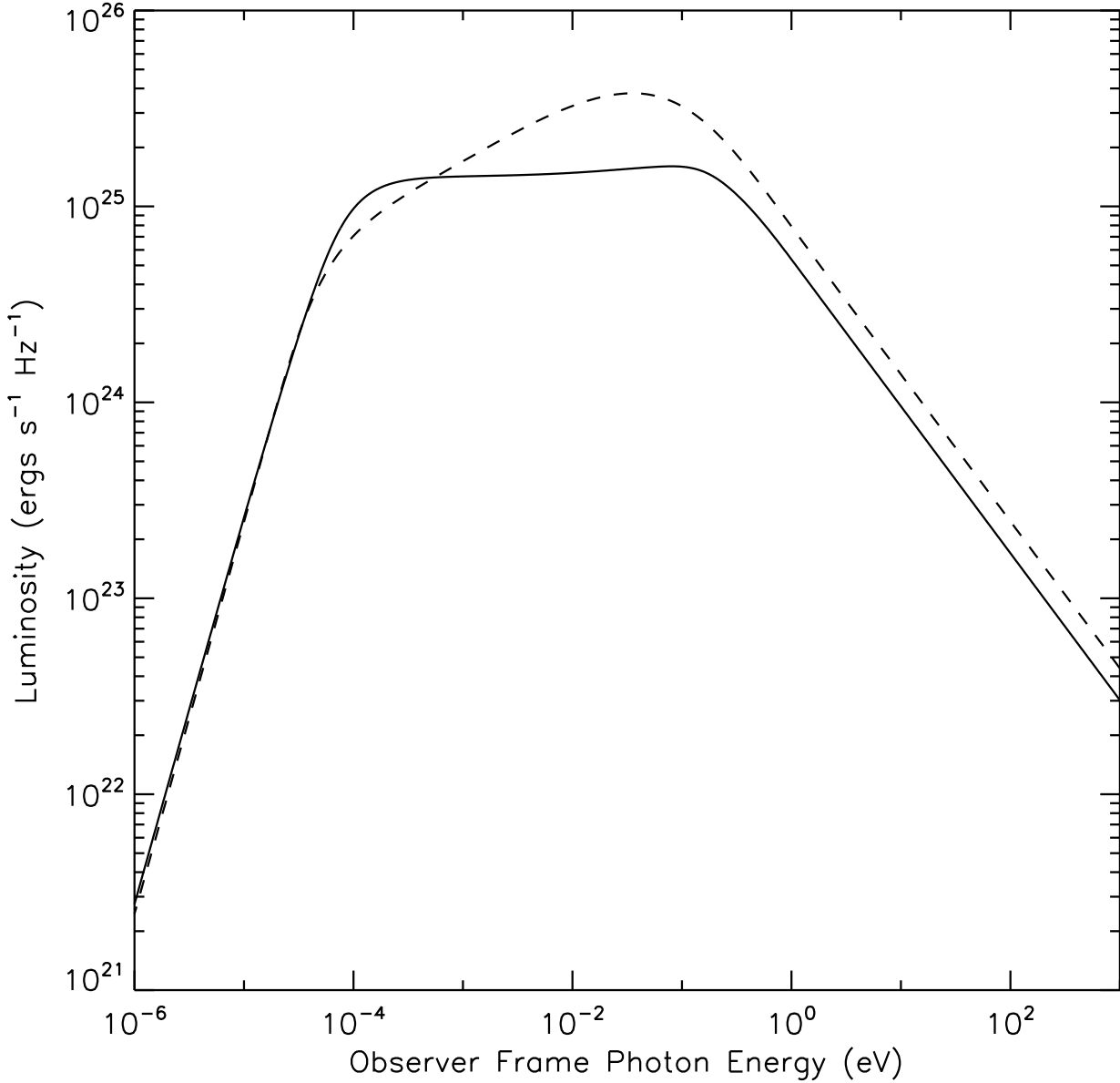


**Figure 7.** The total afterglow power emitted at 1000 s for jitter (solid line) and synchrotron (dashed line) radiation mechanisms under identical conditions. See text for details on the computations.

$(e/\gamma mc)^{\frac{1}{2}} e_{\alpha\beta\gamma} (v_\beta B_\gamma - v_\gamma B_\beta)$ . After simplification this expression results in

$$|\mathbf{w}_{\Omega, \mathbf{k}}|^2 = (ev/\gamma mc)^2 (\delta_{\alpha\beta} - v^{-2} v_\alpha v_\beta) B_{\Omega, \mathbf{k}}^\alpha B_{\Omega, \mathbf{k}}^{*\beta}. \quad (\text{A5})$$

where  $B_{\Omega, \mathbf{k}}^\alpha B_{\Omega, \mathbf{k}}^{*\beta}$  is the Fourier Transform of the field correlation tensor

$$B_{\Omega, \mathbf{k}}^\alpha B_{\Omega, \mathbf{k}}^{*\beta} = TV K_{\alpha\beta}(\Omega, \mathbf{k}) = TV \int e^{i(\Omega t - \mathbf{k} \cdot \mathbf{r})} K_{\alpha\beta}(\mathbf{r}, t) d\mathbf{r} dt, \quad (\text{A6})$$

where  $T$  can be interpreted as the period or duration of emission,  $V$  is the volume integrated over and  $K_{\alpha\beta}(\mathbf{r}, t)$  is the second order correlation tensor of the magnetic field. Using the results above and assuming a time independent magnetic field, equations (A4) and (A5) reduce to

$$\langle |\mathbf{w}_{\omega'}|^2 \rangle = (2\pi V)^{-1} \int |\mathbf{w}_\mathbf{k}|^2 \delta(\omega' + \mathbf{k} \cdot \mathbf{v}) d\mathbf{k}, \quad (\text{A7})$$

$$|\mathbf{w}_\mathbf{k}|^2 = (ev/\gamma mc)^2 (\delta_{\alpha\beta} - v^{-2} v_\alpha v_\beta) V T K_{\alpha\beta}(\mathbf{k}). \quad (\text{A8})$$

The form of  $K_{\alpha\beta}(\mathbf{k})$  used in this paper is taken from numerical simulations of the Weibel Instability and is given by

$$K_{\alpha\beta}(\mathbf{k}) = C(\delta_{\alpha\beta} - n_\alpha n_\beta) f_z(k_\parallel) f_{xy}(k_\perp), \quad (\text{A9})$$

where  $\mathbf{n}$  is the normal to the shock front,  $C$  is proportional to the mean square magnetic field  $\langle B^2 \rangle$ , and  $f_z(k_\parallel)$  and  $f_{xy}(k_\perp)$  describe the structure of the magnetic field parallel and perpendicular to the shocks normal. Inserting

the above into equations (A4) and (A5) and simplifying  $(\delta_{\alpha\beta} - v_\alpha v_\beta/v^2)(\delta_{\alpha\beta} - n_\alpha n_\beta) = 1 + (n_\alpha v_\alpha)^2/v^2 = 1 + \cos^2 \Theta'$ , finally gives the result (for  $v \sim c$ ; Medvedev 2006)

$$\begin{aligned} \langle |\mathbf{w}_{\omega'}|^2 \rangle &= \left(\frac{e}{\gamma m}\right)^2 \frac{CT}{2\pi} (1 + \cos^2 \Theta') \times \\ &\times \int f_z(k_{\parallel}) f_{xy}(k_{\perp}) \delta(\omega' + \mathbf{k} \cdot \mathbf{v}) dk_{\parallel} d^2 k_{\perp}. \quad (\text{A10}) \end{aligned}$$